Atomic force microscopy reveals the assembly of potential DNA "nanocarriers" by poly-L-ornithine

Anita Mann, Meraj Alam Khan, Vasundhara Shukla, Munia Ganguli *

Institute of Genomics and Integrative Biology, Mall Road (near Jubilee Hall), Delhi 110 007, India

Abstract

Atomic force microscopy (AFM) has been used to visualize the process of condensation of plasmid DNA by poly-L-ornithine on mica surface. AFM images reveal that the transition of negatively charged DNA to condensed nanoparticles on addition of increasing amounts of positively charged poly-L-ornithine (charge ratio (Z_+/Z_-) varied between 0.1 and 1) at a wide range of DNA concentrations (3–20 ng/µl) occurs through formation of several distinct morphologies. The nature of the complexes is strongly dependent on both the charge ratio and the DNA concentration. Initiation of condensation when the concentration of DNA is low (~ 3–7 ng/µl) occurs possibly through formation of monomolecular complexes which are thick rod-like in shape. On the contrary, when condensation is carried out at DNA concentrations of 13–20 ng/µl, multimolecular structures are also formed even at low charge ratios. This difference in pathway seems to result in differences in the extent of condensation as well as size and aggregation of the nanoparticles formed at the high charge ratios. To the best of our knowledge, this is the first direct single molecule elucidation of the mechanism of DNA condensation by poly-L-ornithine. Cationic poly-aminoacids like poly-L-ornithine are known to be efficient in delivery of plasmid DNA containing therapeutic genes in a variety of mammalian cell lines by forming condensed "nanocarriers" with DNA. Single molecule insight into the mechanism by which such nanocarriers are packaged during the condensation process could be helpful in predicting efficacy of intracellular delivery and release of DNA from them and also provide important inputs for design of new gene delivery vectors.
© 2007 Elsevier B.V. All rights reserved.

Keywords: DNA condensation; Poly-L-ornithine; Atomic force microscopy; Gene delivery vectors

1. Introduction

The transition of negatively charged DNA from its loose, random coil structure to compact forms like nanoparticles on addition of positively charged ions/molecules is a recurrent theme in biological research since it forms the basis for the fundamental process of DNA condensation [1]. The current interest in DNA condensation arises from the fact that development of non-viral methods for delivering therapeutic genes to the cell involves formation of monodisperse "nanocarriers" (usually nanoparticles) through controlled condensation of plasmid DNA vectors (containing specific genes of interest) by cationic agents [2,3]. A wide multitude of cationic agents (e.g. simple multivalent cations like hexamine cobalt (III), polyamines like spermine and spermidine, cationic silanes, cationic polymers and polypeptides, cationic liposomes etc.) has been shown to condense DNA in vitro [4–7]. It is universally accepted that the cationic agents reduce the intramolecular repulsion among DNA segments, neutralize the negative charges of the phosphate groups on the backbone of DNA molecules, and thereby condense DNA usually into spherical nanoparticles [1]. Many of these cationic agents have been successfully used for preparing condensed DNA nanoparticles for in vitro and in vivo gene delivery [8,9]. Such non-viral nanocarriers do not provoke unexpected immune responses or oncogenic effects due to endogenous virus recombinations (unlike in virus-assisted gene delivery methods) and are thus gaining more attention as gene delivery vectors. The condensed nanoparticles also protect the therapeutic gene

---

in the plasmid against nuclease degradation to ensure enhanced DNA delivery.

Much of the focus of current research in this area has been on finding new, efficient and minimally toxic cationic agents for condensing DNA into nanoparticles and their delivery in eukaryotic cells. Cationic polymers are being explored very extensively in this regard. The condensed polymer-DNA complexes (usually termed as polyplexes) with nanometric dimensions are appropriate for cellular uptake and protected from intracellular enzymatic degradation. While novel cationic polymers modified by ligands (e.g. lactose) for cell-specific receptor-mediated DNA delivery or by hydrophilic moieties like poly(ethyleneglycol) for better water solubility are being designed and synthesized [10,11], achieving high levels of DNA delivery using cationic polymers is still a challenge. One of the possible reasons for this could be that the molecular mechanism by which DNA gets condensed using these agents is not very clearly understood, although it is likely to have important bearing on the stability of the nanoparticles and protected DNA delivery and release. Few studies exist in the literature where efforts have been made to visualize the process of condensation at the single molecule level using atomic force microscopy (AFM) [12–19]. However, many of these reports have used linear DNA molecules for mechanistic elucidation and not the plasmid DNA as a whole. Moreover, the effect of simple parameters like DNA concentration on condensation mechanism at the molecular level has also not been studied systematically from low to high charge ratios although it is expected to play a role in dictating the condensation process.

In this report, we describe the possible mechanism of interaction of cationic polymer poly-L-ornithine (PLO) with plasmid DNA (studied using AFM) as it gets condensed to nanoparticles. Advantages like high resolution visualization of single biomolecules, imaging in air/fluid often under near-physiological conditions etc. make AFM a more versatile tool compared to other conventional microscopic, spectroscopic and light scattering techniques traditionally used to study DNA condensation. PLO is a linear polymer which has been used for intracellular DNA delivery in a variety of cell lines [20,21]. Our aim was to establish the mechanism by which PLO condenses DNA to form DNA nanocarriers. We speculated DNA concentration to be one of the major determinants of the condensation mechanism and hence have also explored the effect of DNA concentration on the condensation process. Complex formation has been examined at charge ratios (Z_+/Z_-) ranging from 0.1 to 1 and DNA concentrations ranging from 3–20 ng/μl. Well-defined structural morphologies formed with increasing charge ratio have been observed. The mechanism of condensation has been found to be strongly dependent on the DNA concentration; it is essentially monomolecular at low DNA concentrations and appears to involve multimolecular condensation also when high DNA concentrations are used. This seems to result in differences in the extent of condensation as well as particle morphology at higher charge ratios. Differences in condensation mechanisms are likely to influence the stability of the DNA nanoparticles carrying the genes of interest in the intracellular medium and the efficiency of their DNA release [2]. Molecular level understanding of the mech-

anism of DNA condensation and the factors controlling the condensation pathways by potential gene delivery agents could thus have an important role to play in designing better gene delivery agents.

2. Experimental

2.1. Chemicals used and plasmid preparation

Poly-L-ornithine (molecular weight 30,000–70,000) was obtained from Sigma Aldrich. pUC19 plasmid (2686 bp in length) was isolated from DH5-α cells using published protocol [22] and its concentration was estimated by uv–visible spectroscopy.

2.2. Preparation of DNA-polymer complexes (polyplex)

Polyplexes with different charge ratios (the ratio of the total positive charges from the cationic polymer to the total negative charges from the DNA (Z_+/Z_-)) were prepared by controlled and slow mixing of equal volumes of DNA and polymer solutions at appropriate concentrations. DNA solutions with concentrations of 6, 14, 26 and 40 ng/μl were prepared from a parent stock solution in water. Polymer stock solutions of varying concentrations were appropriately prepared such that mixing of equal volume of polymer solution with each of the DNA stock solutions would result in formation of polyplexes where the charge ratios varied between 0.1 and 1. Drop-wise addition of DNA solution into the polymer solution with stirring was used to ensure homogeneous mixing as reported in earlier literature [23]. Ten minutes was required in each case for mixing and the total final volume of the mixture was 20 μl. After mixing, the solutions were allowed to stand for a minimum of 30 min before any experiment was carried out. In all the cases, polyplex formation was carried out in water. Four series of solutions were prepared. In each series, the final DNA concentration in the solution was held constant and the charge ratio was varied between 0.1 and 1. The final DNA concentrations in each series were: 3 ng/μl (Series 1), 7 ng/μl (Series 2), 13 ng/μl (Series 3) and 20 ng/μl (Series 4). Solutions with charge ratios of 0.1, 0.25, 0.5, 0.75 and 1 were prepared in each series.

2.3. Gel retardation assay

The electrophoretic mobility of the polyplexes at different charge ratios (Z_+/Z_-) of 0.1, 0.25, 0.5, 0.75 and 1 in each series was studied using agarose gel elctrophoresis. The polyplexes in each series (prepared according to the protocol mentioned above) were loaded into 1% agarose gel containing ethidium bromide. Electrophoresis was carried out at 100 V in TAE buffer for 40 min. DNA bands were visualized under transilluminator.

2.4. Atomic force microscopy

2.4.1. Details of AFM set-up
All AFM images were obtained using a PicoSPM equipment (Molecular Imaging, AZ, USA). Images were obtained in the MAC mode to ensure minimum sample damage. Au–Cr coated

MAC cantilevers (Molecular Imaging), 225 µm long, resonance frequency of 65 kHz and force constant of 2.8 N/m were used for imaging. Scan speed used in most cases was 1 line/s. Topographic images have been presented in all the cases.

2.4.2. Image acquisition details

In order to image free DNA in absence of added PLO, 2 µl of aqueous plasmid DNA solution of 6 ng/µl (to which 2 mM $MgCl_2$ had been added for better visualization of DNA) was deposited on a freshly cleaved piece of mica (1 cm × 1 cm) and allowed to stand for 2 min. The mica was then thoroughly rinsed with a jet of water (about 200 µl was optimal) in order to remove excess DNA and $MgCl_2$ and air-dried. Imaging was immediately carried out in air. This was done in order to measure the dimensions of isolated DNA molecules in absence of PLO (simple deposition in absence of $MgCl_2$ and no washing leads to DNA molecules getting entangled to each other preventing measurement of their actual dimensions). The polyplexes (prepared in water) were imaged by simply depositing 2 µl of the solution on freshly cleaved mica and allowing the aqueous solution to dry in air before imaging. No $MgCl_2$ was used for preparation or visualization of the polyplexes. In each polyplex series where the DNA concentration is kept constant, we have also imaged the bare DNA solution (in absence of added PLO or $MgCl_2$) at that DNA concentration for a comparison of the images in presence and absence of PLO. Care was taken to ensure uniform deposition on the mica surface. Minimum image processing (first order flattening and brightness contrast) was employed in some cases.

2.4.3. Image analysis

For each sample, 15 images (10 µm × 10 µm) were collected for analysis. Initially, the proportion of rod-like, spherical and multimolecular structures in the sample (for details, see Results section) were quantitated by manual counting in order to check for image to image variation. Imaging was repeated with fresh deposition on mica surface whenever there was a variation in the relative proportion of the species by more than 3%. Once it was ascertained that the deposition was uniform and any image can be chosen as a representative one in that series for that particular charge ratio, molecular dimension measurements were done. Image analysis (contour length and width measurements) was carried out using SPIP software. One representative 10 µm × 10 µm image was taken for analysis in each case, containing around 190–220 mol. Predominantly five different molecular morphologies were observed and the molecules were manually categorized based on their shape and dimensions as described in the results section.

3. Results

The experimental approach used here was to allow plasmid DNA (pUC19 has been taken as a model plasmid) to condense gradually in presence of PLO with increasing charge ratios and visualize the intermediates formed in the process. In order to see the effect of DNA concentration on the condensation process, this exercise was undertaken for four series of samples; each

series with a constant DNA concentration, and the charge ratios (Z_+/Z_-) were varied from 0.1 to 1 in each case. All the experiments were carried out in water.

3.1. Gel retardation assay

Agarose gel electrophoresis was carried out in order to look at the condensation process at different charge ratios in the bulk and identify the charge ratios where complete retardation of the DNA bands occur. The images are shown in Fig. 1. While free DNA or incompletely neutralized DNA migrated towards the anode, complete retardation was observed above Z_+/Z_- of 0.75 in Series 1 and Series 2 and at 0.75 in Series 3 and Series 4. This indicates formation of more compact structures when the charge ratio is at or above 0.75 in all the series. It has also been reported in the literature that PLO condenses DNA at a charge ratio less than 1 [24,25]. The marginal difference in the charge ratio where retardation initiates in Series 3 and Series 4 as compared to Series 1 and 2 might be an indication of difference in the amount of condensed species present in the two cases at this charge ratio. However, the morphology of the structures formed during the process of condensation cannot be determined from gel electrophoresis. We do not observe any difference in the rate of migration of partly charge compensated DNA at charge ratio of 0.1, 0.25 etc. although loosely complexed DNA is likely to be present at lower charge ratio. Hence AFM was carried out at different charge ratios in each series of samples to identify these morphologies and the results are described below.
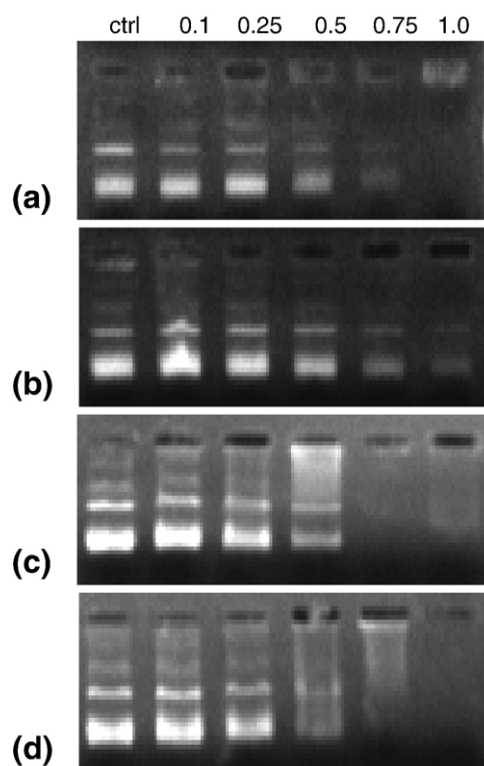

Fig. 1. Electrophoretic mobility shift assay of the polyplexes on 1% agarose gel. Control plasmid DNA is loaded in lane 1, lane 2–6 contain polyplexes formed at different charge ratios (as mentioned in the figure) (see Experimental section for details).
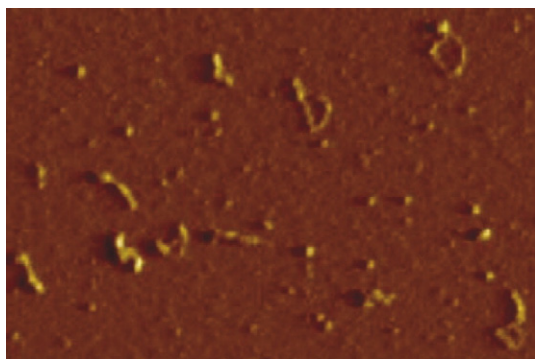
Fig. 2. AFM image of pUC19 molecules. Scan range: 2.1 μm × 3.5 μm.

3.2. Atomic force microscopy

3.2.1. Images of bare DNA

Fig. 2 shows a representative AFM image of bare pUC19 DNA molecules on mica surface in the absence of any PLO. Mg^{2+} ions were used optimally in order to facilitate the adhesion of DNA on to mica for best viewing [26]. The contour length,
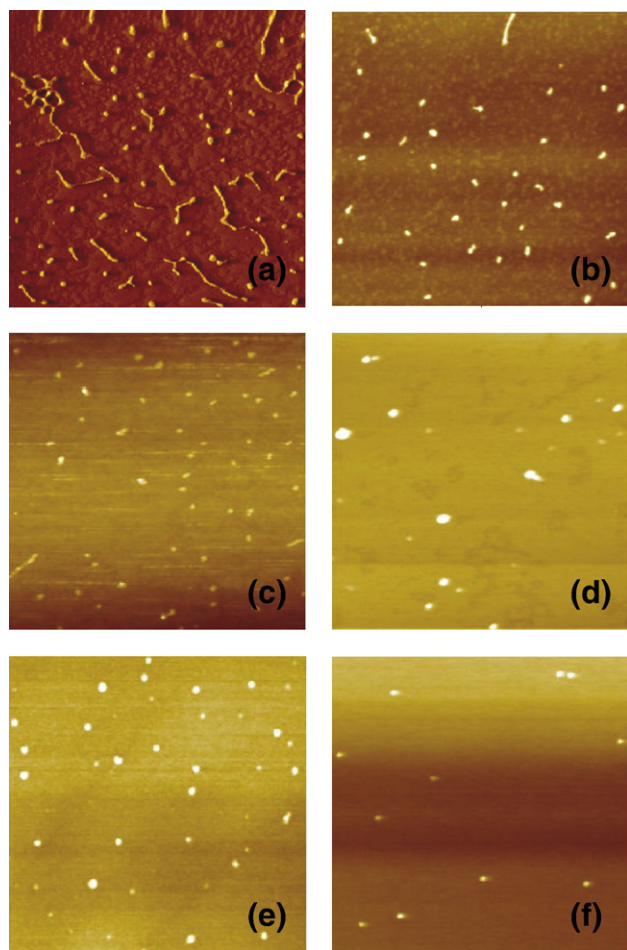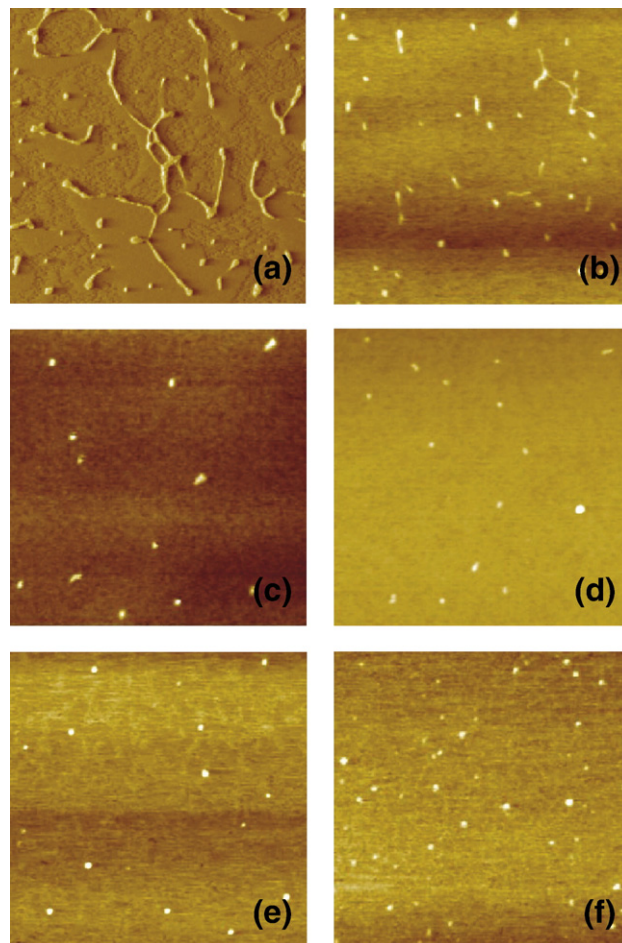

Fig. 3. Representative AFM images of DNA-PLO complexes (Series 1). DNA concentration is fixed at 3 ng/μl (a) charge ratio 0.0 (b) charge ratio 0.1 (c) charge ratio 0.25 (d) charge ratio 0.5 (e) charge ratio 0.75 (f) charge ratio 1. All images are 4 μm × 4 μm in size.

Fig. 4. Representative AFM images of DNA-PLO complexes (Series 2). DNA concentration is fixed at 7 ng/μl. (a) charge ratio 0.0 (b)charge ratio 0.1 (c) charge ratio 0.25 (d) charge ratio 0.5 (e) charge ratio 0.75 (f) charge ratio 1. All images are 4 μm × 4 μm in size.

width and height of 50 tightly supercoiled molecules were analyzed. The results show that the average height of the molecules is about 1.3 ± 0.2 nm which is twice that of double stranded DNA molecules (0.6 ± 0.1 nm) as reported in the literature [27,28]. The width of these tightly supercoiled molecules is about 20 ± 2 nm, and the contour lengths are 340 ± 30 nm which are also consistent with earlier reports [29].

3.2.2. Images of DNA-PLO complexes

Fig. 3 shows the AFM images of the DNA molecules in progressive stages of compaction as the charge ratio is increased from 0 to 1. The DNA concentration is kept constant here at 3 ng/μl (Series 1). Similar images of DNA molecules in successive stages of condensation are seen in Fig. 4 (DNA concentration held constant at 7 ng/μl, Series 2), Fig. 5 (DNA concentration 13 ng/μl, Series 3) and Fig. 6 (DNA concentration 20 ng/μl, Series 4). The molecular architectures vary significantly from that of bare plasmid DNA and molecules of different shape and size are seen at each charge ratio in each series. However, upon carefully analyzing the images from all the series of samples at all the charge ratios and measuring the
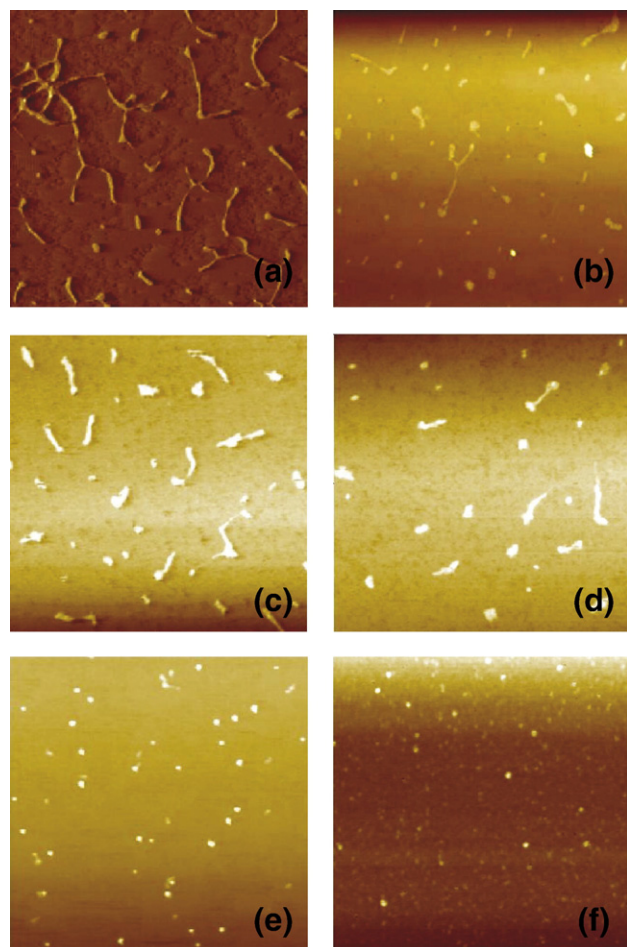
Fig. 5. Representative AFM images of DNA-PLO complexes (Series 3). DNA concentration is fixed at 13 ng/μl. (a) charge ratio 0.0 (b)charge ratio 0.1 (c) charge ratio 0.25 (d) charge ratio 0.5 (e) charge ratio 0.75 (f) charge ratio 1. All images are 4 μm×4 μm in size.

molecular dimensions, predominantly five different molecular morphologies were detected. These are put together in Table 1 along with representative images of each type of species. The proportions of these different molecules vary at each charge ratio within one series and also differ from series to series at similar charge ratios. The population distribution of these different species seen at different Z_+/Z_- in each of the series is shown in Fig. 7. Around 200 molecules were taken in each case for the analysis.

At charge ratio of 0 (free DNA) in Series 1, the DNA molecules seem to be entangled to each other forming networks and clusters of different shapes. Once PLO is present at a low charge ratio of 0.1 and 0.25 in Series 1 (DNA concentration 3 ng/ μl), which are the farthest from the charge neutralization conditions, the predominant morphologies seen are thick and very short rods (70–120 nm in length, 50–70 nm in width, category 3 in Table 1) as seen in Fig. 3b and c. Majority of them look nearly oval in shape. A substantial fraction of the molecules are somewhat longer rod-like structures (120–200 nm in length and 40–60 nm in width, category 2 in Table 1). The width variations mentioned here are in some cases within a single

molecule also. Spheres (30–60 nm in diameter, see category 5 in Table 1) are low in number. There are very few structures in which multiple DNA molecules seem to have clustered together (category 4 in Table 1). With increasing charge ratio, there is an increase in the proportion of more condensed spherical structures which are 30–60 nm in diameter (note that in few cases the spheres look mildly distorted; all such structures are also included in category 5) while the proportion of rod-like structures significantly drop down (see Fig. 3(d) and (e)). At the highest charge ratio of 1 examined in this study, majority of the molecules are spherical as seen in Fig. 3f, as well as Fig. 7(a). In case of Series 2 (DNA concentration 7 ng/μl), the nature of the molecules as well as the progressive changes in their morphology with increasing charge ratio is quite similar to that observed in Series 1 as is evident from Figs. 4 and 7(b). Condensation seems to proceed through formation of rod-like structures of different dimensions which gradually condense to spherical structures at higher charge ratios. There are very few structures (about 4–7%) in both the series which seem to have formed by association of multiple DNA molecules (see Fig. 7(a) and (b)).

However, there is a marked change in the trend in case of Series 3 and Series 4 where the DNA concentrations are 13 and
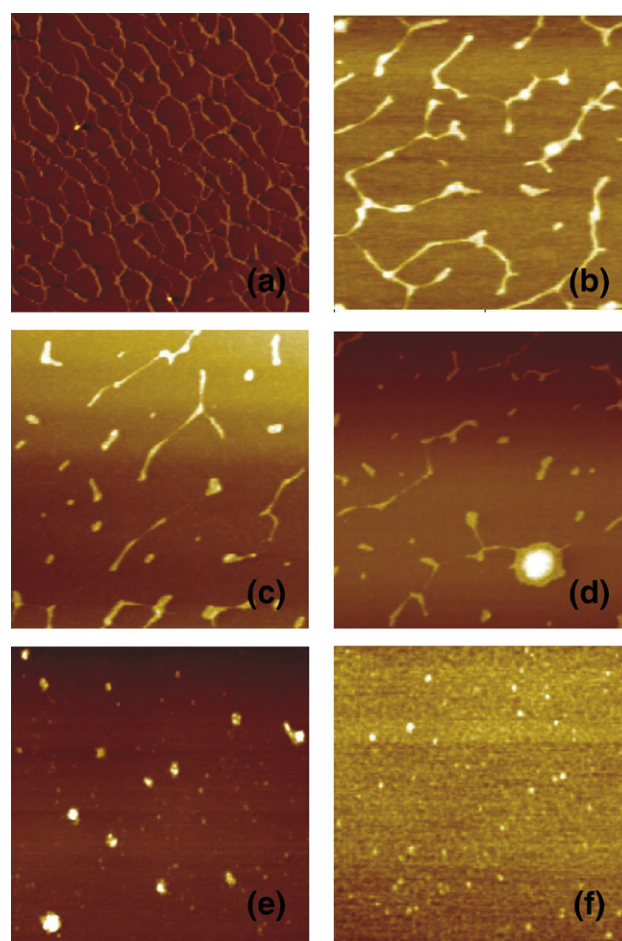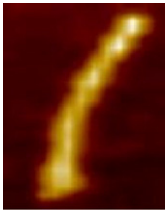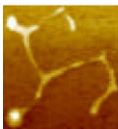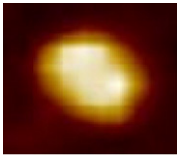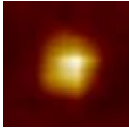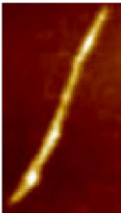

Fig. 6. Representative AFM images of DNA-PLO complexes (Series 4). DNA concentration is fixed 20 ng/μl. (a) charge ratio 0.0 (b) charge ratio 0.1 (c) charge ratio 0.25 (d) charge ratio 0.5 (e) charge ratio 0.75 (f) charge ratio 1. All images are 4 μm×4 μm in size.

Table 1
Different molecular morphologies present in all the series of samples at different charge ratios

Category	Representative AFM image	Category	AFM image
1) Rod, linear length: 200–350 nm width: 20–40 nm		4) Multimolecular long rods: length: 350–700 nm, width 20–80 nm, Multiple molecule network, flower-like spheres	
2) Rod, linear length: 120–200 nm width: 40–60 nm		5). Spheres 30–60 nm in diameter, distorted spheres of length 50–60 nm and width 30–50 nm	
3). Thick rod (oval shaped) length: 70–120 nm width: 50–70 nm			

20 ng/μl respectively. In both these series, at low charge ratios, one does see rod-like structures of dimensions similar to those seen in the corresponding similar charge ratios in Series 1 and 2 in addition to longer rods (200–350 nm in length and 20–40 nm in width, category 1 in Table 1). However, the major distinguishing feature is the presence of a large number of structures at low charge ratios of 0.1 and 0.25 in which several DNA molecules seem to be joining together (see Figs. 5 and 6(b) and (c)). Such structures are rarely visible in Series 1 and Series 2, and contribute significantly at low charge ratios in Series 3 and Series 4. In fact, images from charge ratio of 0.1 in Series 4 show a large number of interconnected DNA molecules forming almost a network on the mica surface as seen in Fig. 6(b). This makes it difficult to actually measure the dimensions of individual species, and hence the data of 0.1 is not represented in Fig. 7(c) and (d) for both Series 3 and Series 4. The presence of these species is a strong indication of condensation progressing via formation of multimolecular species also in these cases. On increasing the charge ratio to 0.5, there is a sharp drop in the proportion of the linear multimolecular structures. Instead, some spherical structures which often show DNA strands around a central node are visible, along with a large number of rod-like structures of varying dimensions (i.e. those belonging to category 1, 2 and 3 of Table 1). More spherical, distorted spherical as well as aggregated spheres are seen at higher charge ratios of 0.75 and 1 (see Figs. 5 and 6(d) and (e)). It is also worth noting that there is a significant proportion of molecules belonging to Category 3 in charge ratio 1 of both Series 3 and Series 4. In fact, in Series 3 and Series 4 there is about 30% drop in the proportion of nanoparticles and corresponding increase in the small rod-like structures (category 3 of Table 1) with increase in the charge ratio from 0.75 to 1. This is in sharp

contrast with the situation in Series 1 and Series 2 where the proportion of the nanoparticles either increases or decreases marginally (about 10%) as the charge ratio increases from 0.75 to 1. We have tried to rationalize this observation in the discussion section. Additionally, we have checked the size distribution of the nanoparticles (belonging to category 5 of Table 1) formed at charge ratios of 0.75 and 1 in all the four Series. The results are shown in Fig. 8, along with the proportion of molecules belonging to category 3 (thick rods, since these are also seen at the highest charge ratios). It is seen that in Series 3 and Series 4, at charge ratio 0.75, majority of the particles are in the size range of 30–45 nm and there are very few which are 50–60 nm in diameter. This is in contrast with the situation at charge ratio 1 where majority of the nanoparticles are 50–60 nm in size. In Series 1 and 2, however, particles of both 30–45 nm in size as well as 50–60 nm in size are present in both charge ratio 0.75 and charge ratio 1.

4. Discussion

4.1. Importance of studying DNA condensation mechanism

Size and shape of nanocarriers formed by controlled condensation of DNA and thermodynamics of DNA condensation using many classes of cationic agents has been studied in vitro [1]. However, except in some isolated instances, little attention has been given towards identifying the structural intermediates involved during the condensation process at the single molecule level and thereby delineating condensation pathways [30]. AFM has been elegantly used to visualize the folding pathway of spermidine-induced condensation of DNA by varying the amount of added spermidine in a dilute DNA solution where reduction of DNA
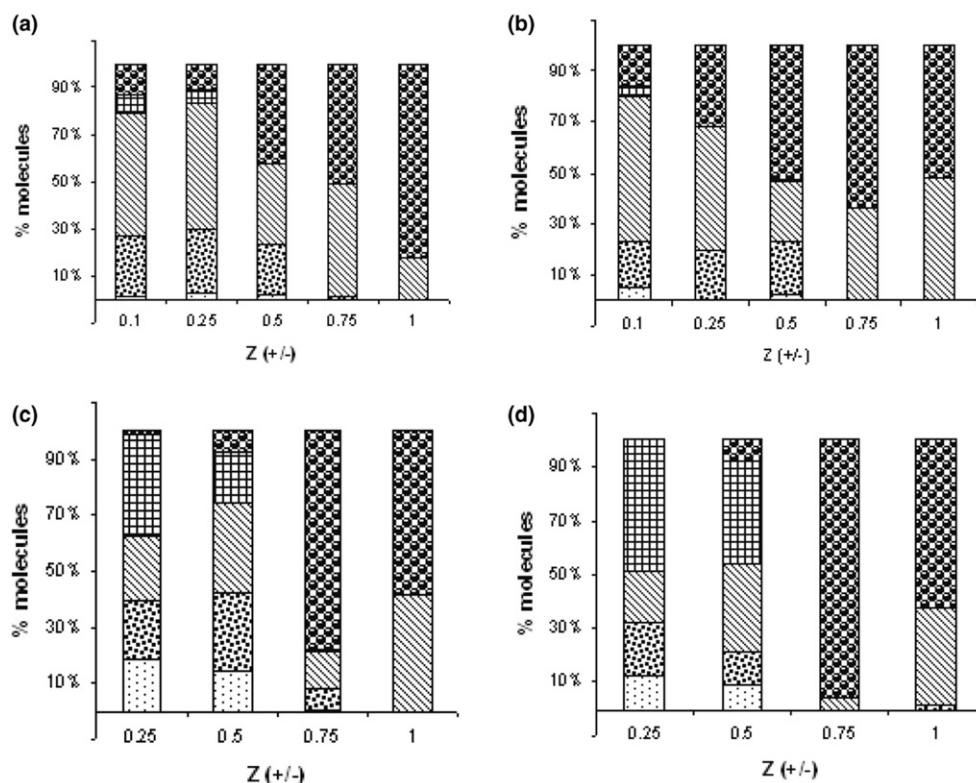
Fig. 7. Population distribution of the different categories of molecules in each series at different charge ratios. Each symbol in the figure represents one category of molecules (see Table 1) according to the following scheme: ▨ 1 ▧ 2 ▨ 3 ▦ 4 ▨ 5 where 1 = Rod, linear (200–350 nm), 2 = Rod, linear (120–200 nm), 3 = thick rod (70–120 nm), 4 = multimolecular (linear and spherical), 5 = spheres and distorted spheres (30–60 nm). Analysis was done as described in the experimental section. 190–220 molecules were counted for each image at each charge ratio in all the series (exact number depending upon the number of molecules seen in a representative 10 μm × 10 μm image). Relative proportions were then calculated as percentages.

persistence length, loop formation, crossover stabilization, multimerization and strand-strand stabilization have been identified as the different steps involved [12]. Similarly cryogenic electron microscopy has identified spermine/uranyl–salt-induced condensates of DNA [31]. However, such studies are few and most of them use linear DNA. Further, for mechanistic elucidations, near neutralization concentrations of the cationic agents have been

Fig. 8. Particle size distribution of the nanoparticles formed at charge ratio of 0.75 and 1 in all the Series. ▨ Spheres: 30–45 nm ▨ Spheres: 50–60 nm ▨ Thick rods, category 3 (70–120 nm length, 50–70 nm width).

used. It is imperative to understand packaging mechanisms and the factors which control the same because it is likely to have a direct correlation with the stability of the condensation products and their intracellular un-packaging. In fact, the importance of controlling condensation of DNA containing functional genes has been highlighted in some of the recent investigations where the transfection efficiency in vitro and in vivo have been correlated to the packaging of DNA [32,9]. Some attempts have been made towards establishing better structure-activity correlations in case of DNA-nanoparticles formed with cationic polymers and their gene delivery properties [33–35], where the effect of polymer structure, its size and shape and its chemical properties have been looked into. Such studies, however, have not explored the pathway(s) which are followed as DNA condenses into nanoparticles.

We believe that the degree of condensation and the mechanism will definitely have a role to play in the effectiveness of a complexed nanocarrier to deliver the therapeutic gene. The balance between compact binding and efficient release is the hallmark of good DNA delivery agents and would be dictated by the manner in which the nanocarrier is packaged. Understanding the factors controlling the packaging mechanism would be a necessary step towards that direction. With this objective in mind, we have tried to identify the unique structural morphologies which are formed as plasmid DNA condenses in presence of PLO and the effect of DNA concentration on the mechanism of DNA condensation.
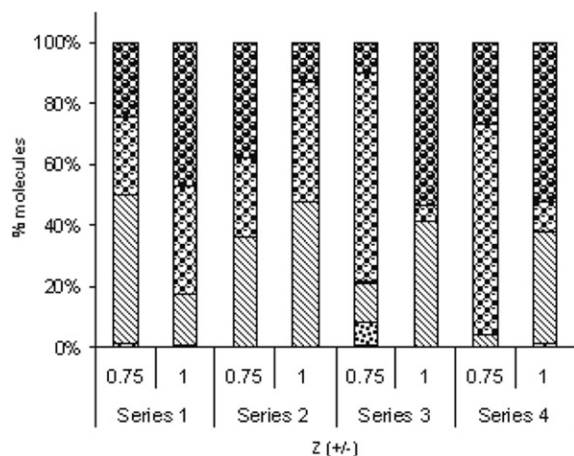
4.2. Revealing the possible mechanism of condensation

Our experiments give valuable insight into the mechanism of condensation of plasmid DNA by PLO. Although there is a distribution of different types of molecular structures at each charge ratio for all the four series examined here as seen in Figs. 3–7, there seems to be a distinct trend in the mechanism by which DNA is packaged with increasing amount of PLO in each series. Since the polyplex formation has been carried out in the absence of any buffer, role of extraneous factors (e.g. presence of Mg^{2+}) on the condensation process can be ruled out, and the morphologies seen are arising from condensation of DNA by PLO. Furthermore, although there is a possibility that the different morphologies formed at each charge ratio might have differential binding affinity to the mica surface because of different surface charges, our imaging protocol (which does not involve any washing step)

effectively rules out the possibility of visualizing only those structures which adsorb relatively strongly on the surface. We have tried to analyze the mechanism of DNA condensation by assuming that the structures seen on the mica surface in each condition are the ones that are actually present in the solution.

The morphologies are quite distinct in each series and DNA concentration is one of the determinants of the mechanism of condensation as speculated. It also seems intuitively clear that the mechanism of condensation is monomolecular at low DNA concentrations while there is also a multimolecular component at higher DNA concentrations. Based on this observation, we have tried to propose a possible mechanism for condensation (shown as a schematic in Fig. 9) of the different series as described below.

It has been mentioned already that in Series 1 (where the DNA concentration is very low), condensation starts at low charge ratios of 0.1 by predominant formation of rod-like structures of
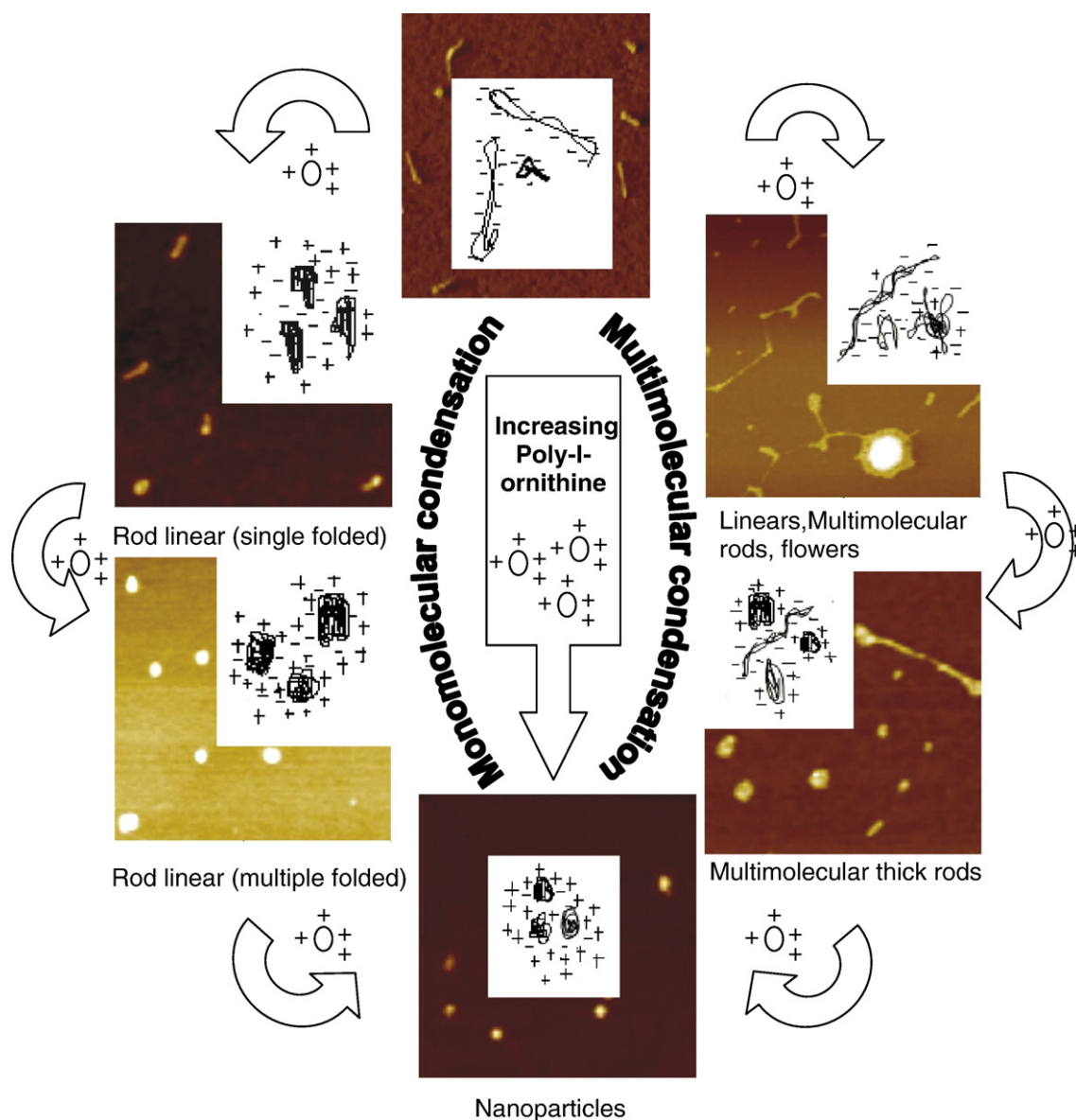

Fig. 9. Schematic representing the proposed mechanism of condensation of plasmid DNA with poly-L-ornithine at high (13–20 ng/μl) and low DNA (3–7 ng/μl) concentrations. Monomolecular condensation is seen at low DNA concentration whereas both monomolecular and multimolecular condensation is seen at high DNA concentrations.

different sizes. These features are quite distinct from the DNA molecules seen in absence of PLO (Fig. 3(a)). Although the rod-like structures have different dimensions, one common feature is that in all the cases, their lengths are less than that of the individual supercoiled plasmid molecules, while their widths are higher. This seems to indicate that these are formed from condensation of individual plasmid molecules and are thus likely to be monomolecular in nature. We speculate that one of the possible ways by which such structures might have originated is by bending and folding of individual plasmid molecules in presence of cationic PLO which neutralizes the repulsion among DNA double strands and allow them to come closer. Such a bending process might be repeated in presence of increasing proportion of condensing agent, i.e. a single folded plasmid molecule which forms a thick rod-like structure can further bend and fold to generate a smaller and thicker rod-like structure through multiple folding as shown in Fig. 9. The large length and width distribution in the molecules seen at initial stages of condensation could be because of such multiple folding and varying degrees of condensation and this can account for the presence of molecules in category 1, 2 and 3 in varying proportions in the lower charge ratios of Series 1. Bending of plasmid DNA during condensation has been observed for other cationic agents also [15]. Occasionally, toroidal structures are seen in the images which seem to be have generated from bending of the rods where the two ends have joined. These are, however, very few and hence have not been included in any category in Table 1. As the charge ratio increases to 1, spherical particles ($\sim$ 30–60 nm in diameter) which are likely to have formed from repeated bending and folding of DNA in presence of PLO (generating molecules of category 2 and 3, see Table 1) followed by further condensation are the predominant species, although the very short and thick rod-like structures (category 3 in Table 1) are still present. Thus the systematic reduction in dimensions of the rod-like and globular features with increasing charge ratio is indicative of the fact that they are arising out of condensation of DNA by bending and folding of the DNA molecules. Increase in the proportion of nanoparticles with increasing charge ratio also indicates very clearly that these species are originating from PLO-induced DNA condensation.

AFM images at different charge ratios in Series 2 show a trend very similar to that seen in Series 1. This seems to indicate that increasing the overall DNA concentration from 3 ng/µl to 7 ng/µl does not have any major effect on the packaging pathway. However, when the DNA concentration is increased to 13 ng/µl as in Series 3, a large number of structures are formed by multimolecular association, indicating that multimolecular condensation pathways also exist as depicted in Fig. 9. The existence of multimolecular structures are manifest not only as entangled molecules, but also as individual molecules which are longer than 350 nm (i.e. more than the plasmid length) and widths in the range of 20–80 nm (higher width than the plasmid molecules). These are likely to have arisen from side by side and/or end-to-end association of the plasmid molecules. In fact, since a large part of the DNA molecules are condensing multimolecularly at low charge ratios in Series 3 and Series 4 utilizing most of the PLO, the remaining species present are usually the less condensed longer rods (category 1 in Table 1, possibly formed by single folding of

plasmid molecules) in which little PLO has been used for condensation. We rarely see these once-folded rods at the low charge ratios in Series 1 and Series 2 (as seen in Figs. 3(b) and 4(b)). The other feature is that at charge ratios of 0.25 and 0.5 of Series 3 and Series 4, one also sees flower-like structures with DNA strands surrounding a central nodal region. The morphology indicates that these are multimolecular in nature and are formed as condensation progresses further. As the charge ratio is increased, both these multimolecular and monomolecular products are further condensed to nanoparticles. At charge ratio of 0.75, near-complete condensation occurs in both these series as indicated by the predominant presence of spherical structures at this charge ratio. The morphology of these nanoparticles formed at charge ratio 0.75 and 1 are somewhat different from those seen in Series 1 and 2: they are more distorted in shape and show strong aggregation tendencies.

The consequences of these differences in the packaging mechanism are manifested at the high charge ratios in several ways. First of all, it should be noted that in Series 1 and Series 2, the proportion of spherical particles at charge ratio 0.75 is much lower as compared to Series 3 and Series 4 (see Fig. 7, molecules in category 5). This seems to indicate that when both monomolecular and multimolecular mechanisms are operative, more number of condensed nanoparticles form at a lower charge ratio itself. This is also indicated in the agarose gel experiments where retardation of the DNA band occurs from 0.75 onwards in Series 3 and Series 4 while in Series 1 and 2, DNA bands are still visible at charge ratio 0.75. Secondly, the proportion of nanoparticles increases or drops very marginally in Series 1 and Series 2 as the charge ratio increases from 0.75 to 1. This is in sharp contrast with the large decrease (about 30%) in the proportion of nanoparticles at charge ratio 1 as compared to charge ratio 0.75 in case of Series 3 and Series 4. A possible reason for this could be that in Series 3 and 4, since proportion of fully condensed species (nanoparticles) is already very high at charge ratio 0.75, further addition of the cationic agent leads to aggregation of the nanoparticles. This results in formation of molecular architectures which are of similar dimensions as those seen in category 3, although they are actually originating by a different process, i.e. from aggregation of nanoparticles at charge ratio 1. In fact, aggregation is seen even at charge ratio of 0.75 in these series, although here the particles can be distinguished separately and can be counted as individual nanoparticles unlike in charge ratio 1.

This effect is also manifest in the nanoparticle size. Nanoparticles formed at charge ratio 0.75 and 1 in all the series are in the range of 30–60 nm in diameter. However, if one carefully analyzes the proportion of the particles in the range 30–45 nm and those which are 50–60 nm in diameter in all the series as shown in Fig. 8, it is clear that majority of the particles are in 50–60 nm range in case of Series 3 and Series 4 as compared to Series 1 and Series 2 at charge ratio 1. Thus it seems that although occurrence of multimolecular condensation at high DNA concentrations results in formation of nanoparticles even below charge neutralization conditions, particle sizes are higher probably because of increased DNA content in these cases where multimolecular condensation mechanism is also operative. Increasing the charge ratio also leads to increase in aggregation

which changes the morphology of the condensed species. This might have important consequences on the DNA delivery as well as release characteristics of the formulations prepared under high DNA concentration and high charge ratios. Our basic study could pave way for further detailed investigation on PLO-induced DNA condensation in physiological conditions and its impact on nanoparticle stability, release characteristics and transfection efficiency.

4.3. Reasons for choosing poly-L-ornithine (PLO)

PLO is one of the earliest poly amino-acids used for transfection [20,21] in a variety of cell lines and is one of the model polymers which can be used for understanding DNA condensation. Gene transfer vectors formed between cationic PLO and plasmid DNA have demonstrated superior transfection efficiency (over other such similar polymers like poly-L-lysine) and are more stable to disruption by polyanions like poly-L-aspartic acid [24,25]. It has also been shown in the literature that cationic peptides based on ornithine and histidine form efficient building blocks for non-viral gene transfer [36]. PLO is a linear polymer with simple architecture; understanding DNA condensation mechanism using a model system like PLO would pave the way for further such studies with other polymers and peptides of different chemistry and more complicated architecture.

4.4. Other considerations

It should also be mentioned here that in this study, DNA molecules have been moved along one or more condensation pathways by gradually increasing the concentration of the condensing agent PLO and the imaging has been carried out in air on mica surface. While this provides very meaningful information on the types of molecular architecture formed at different charge ratios and allows us to draw inference on the mechanism of packaging, they do not provide information on the time-resolved evolution of partially condensed structures in fluid which eventually lead to the formation of nanoparticles. Thus the structures that we see here in each series with increasing charge ratios are the thermodynamically stable structures formed at these charge ratios and may or may not represent the kinetic intermediates formed as DNA assembles in presence of charge-compensating amount of polycation. Such study of real-time dynamics of evolution of DNA condensates [37–39] carried out using fluid imaging in buffers of physiological relevance would not only give further insight into the process of condensation of plasmid DNA but also give more input into their importance in biological context. Such work is underway in our laboratory.

Furthermore, it is seen here that the DNA condensation pathways vary depending upon the DNA concentration and that has a bearing on the extent of condensation, particle size, aggregation, as well as the nature of the condensed species formed at high charge ratios. We have not explored the consequence of this difference in packaging mechanism on the stability and DNA release properties of these nanocarriers formed at high charge ratios in relation to in vitro gene delivery, although it is intuitively clear that nanoparticles packaged

through different mechanisms will vary in their stability and efficacy of DNA release. Such studies are also underway in our laboratory.

5. Conclusion

This study involves visualization of the different morphologies formed as plasmid DNA is condensed by poly-L-ornithine using atomic force microscopy. The nature of these morphologies is dependent on the charge ratio and DNA concentration. Condensation seems to be essentially monomolecular when low DNA concentrations are used and involve multimolecular condensation also at high DNA concentration. This affects the extent of condensation, particle size and particle aggregation properties. Such structural views of the condensates, including their dimensions and method of packing could help in better design of DNA delivery vectors.

Acknowledgements

References

[1] V.A. Bloomfield, DNA condensation, Curr. Opin. Struck. Biol. 6 (1996) 334–341.

[2] V. Vjayanathan, T. Thomas, T.J. Thomas, DNA nanoparticles and development of DNA delivery vehicles for gene therapy, Biochemistry 41 (2002) 14085–14094.

[3] S.D. Patel, D.G. Rhodes, D.J. Burgess, DNA-based therapeutics and DNA delivery systems: a comprehensive review, AAPS J. 7 (2005) E61–E77.

[4] D. Luo, W.M. Saltzman, Synthetic DNA delivery systems, Nat. Biotechnol. 18 (2000) 33–37.

[5] J. Widom, R.L. Baldwin, Cation-induced toroidal condensation of DNA studies with Co(NH$_3$)$_6^{3+}$, J. Mol. Biol. 144 (1980) 431–453.

[6] V. Vijayanathan, T. Thomas, A. Shirahata, T.J. Thomas, DNA condensation by polyamines: a laser light scattering study of structural effects, Biochemistry 40 (2001) 13644–13651.

[7] V. Vijayanathan, T. Thomas, T. Antony, A. Shirahata, T.J. Thomas, Formation of DNA nanoparticles in the presence of novel polyamine analogues: a laser light scattering and atomic force microscopic study, Nucleic Acids Res. 32 (2004) 127–134.

[8] M. Ohsaki, T. Okuda, A. Wada, T. Hirayama, T. Niidome, H. Aoyagi, In vitro gene transfection using dendritic poly(L-lysine), Bioconjug. Chem. 13 (2002) 510–517.

[9] J.C. Perales, G.A. Grossmann, M. Molas, G. Liu, T. Ferkol, J. Harpst, H. Oda, R.W. Hanson, Biochemical and functional characterization of DNA complexes capable of targeting genes to hepatocytes via the asialoglycoprotein receptor, J. Biol. Chem. 272 (1997) 7398–7407.

[10] Y.H. Choi, F. Liu, J.S. Park, S.W. Kim, Lactose-poly(ethyleneglycol)-grafted poly-L-lysine as hepatoma cell-targeted gene carrier, Bioconjug. Chem. 9 (1998) 708–718.

[11] C.-H. Ahn, S.Y. Chae, Y.H. Bae, S.W. Kim, Synthesis of biodegradable multi-block copolymers of poly(L-lysine) and poly(ethyleneglycol) as non-viral gene carrier, J. Control. Release 97 (2004) 567–574.

[12] Y. Fang, J.H. Hoh, Early intermediates in spermidine-induced DNA condensation on the surface of mica, J. Am. Chem. Soc. 120 (1998) 8903–8909.

[13] Y. Fang, J.H. Hoh, Cationic silanes stabilize intermediates in DNA condensation, FEBS Lett. 459 (1999) 173–176.

[14] D.D. Dunlap, A. Maggi, M.R. Soria, L. Monaco, Nanoscopic structure of DNA condensed for gene delivery, Nucleic Acids Res. 25 (1997) 3095–3101.

[15] R. Golan, L.I. Pietrasanta, W. Hsieh, H.G. Hansma, DNA toroids: stages in condensation, Biochemistry 38 (1999) 14069–14076.

[16] M.J. Allen, E.M. Bradbury, R. Balhorn, AFM analysis of DNA-protamine complexes bound to mica, Nucleic Acids Res. 25 (1997) 2221–2226.

[17] H.G. Hansma, R. Golan, W. Hsieh, C.P. Lollo, P. Mullen-Ley, D. Kwoh, DNA condensation for gene therapy as monitored by atomic force microscopy, Nucleic Acids Res. 26 (1998) 2481–2487.

[18] Z. Lin, C. Wang, X. Feng, M. Liu, J. Li, C. Bai, The observation of the local ordering characteristics of spermidine-condensed DNA: atomic force microscopy and polarizing microscopy studies, Nucleic Acids Res. 26 (1998) 3228–3234.

[19] I. Goessl, L. Shu, A.D. Schlueter, J.P. Rabe, Molecular structure of single DNA complexes with positively charged dendronized polymers, J. Am. Chem. Soc. 124 (2002) 6860–6865.

[20] V.C. Bond, B. Wold, Poly-L-ornithine-mediated transformation of mammalian cells, Mol. Cell. Biol. 7 (1987) 2286–2293.

[21] Y. Dong, A.I. Skoultchi, J.W. Pollard, Efficient DNA transfection of quiescent mammalian cells using poly-L-ornithine, Nucleic Acids Res. 21 (1993) 771–772.

[22] F.M. Ausubel, R. Brent, R. Kingston, D. Moore, J. Seidman, J.A. Smith, K. Struhl, Current Protocols in Molecular Biology, John Wiley and Sons, New York, 1994, p. 185.

[23] M. Molas, R. Bartons, J.C. Perales, Single-stranded DNA condensed with poly-L-lysine results in nanometric particles that are significantly smaller, more stable in physiological ionic strength fluids and afford higher efficiency of gene delivery than their double-stranded counterparts, Biochim. Biophys. Acta 1572 (2000) 37–44.

[24] E. Ramsay, J. Hadgraft, J. Birchall, M. Gumbleton, Examination of the biophysical interaction between plasmid DNA and the polycationis, polylysine and polyornithine, as a basis for their differential gene transfection in-vitro, Int. J. Pharm. 210 (2000) 97–107.

[25] E. Ramsay, M. Gumbleton, Polylysine and polyornithine gene transfer complexes: a study of complex stability and cellular uptake as a basis for their differential in vitro transfection efficiency, J. Drug Target 10 (2002) 1–9.

[26] H.G. Hansma, M. Bezanilla, F. Zenhausern, M. Adrian, R.L. Sinsheimer, Atomic force microscopy of DNA in aqueous solutions, Nucleic Acids Res. 21 (1993) 505–512.

[27] H.G. Hansma, I. Revenko, K. Kim, D.E. Laney, Atomic force microscopy of long and short double stranded, single-stranded and triple-stranded nucleic acids, Nucleic Acids Res. 24 (1996) 713–720.

[28] A. Schaper, J.P. Pascual Starink, T.M. Jovin, The scanning force microscopy of DNA in air and in n-propanol using new spreading agents, FEBS Lett. 355 (1994) 91–95.

[29] L.H. Pope, M.C. Davies, C.A. Laughton, C.J. Roberts, S.J.B. Tendler, P.M. Williams, Intercalation-induced changes in DNA supercoiling observed in real-time using atomic force microscopy, Anal. Chim. Acta 400 (1999) 27–32.

[30] B.J. Rackstraw, A.L. Martin, S. Stolnik, C.J. Roberts, M.C. Garnett, M.C. Davies, S.J.B. Tendler, Microscopic investigations into PEG-cationic polymer-induced DNA condensation, Langmuir 17 (2001) 3185–3193.

[31] C. Boettcher, C. Endisch, J.-H. Fuhrhop, C. Catterall, M. Eaton, High-yield preparation of oligomeric C-type DNA toroids and their character-ization by cryoelectron microscopy, J. Am. Chem. Soc. 120 (1998) 12–17.

[32] T. Niidome, N. Ohmori, A. Ichinose, A. Wada, H. Mihara, T. Hirayama, H. Aoyagi, Binding of cationic alpha-helical peptides to plasmid DNA and their gene transfer abilities in cells, J. Biol. Chem. 272 (1997) 15307–15312.

[33] M.X. Tang, F.C. Szoka, The influence of polymer structure on the interactions of cationic polymers with DNA and morphology of the resulting complexes, Gene Ther. 4 (1997) 823–832.

[34] M. Maennisto, S. Vanderkerken, V. Toncheva, M. Elomaa, M. Ruponen, M. Schacht, A. Urtti, Structure-activity relationships of poly(L-lysines): effects of pegylation and molecular shape on physicochemical and biological properties in gene delivery, J.Control. Release 83 (2002) 182.

[35] S.E. Eldred, M.R. Pancost, K.M. Otte, D. Rozema, S.S. Stahl, S.H. Gellman, Effects of side chain configuration and backbone spacing on the gene delivery properties of lysine-derived cationic polymers, Bioconjug. Chem. 16 (2005) 694–699.

[36] S.P. Chamarthy, J.R. Kovacs, E. McClelland, D. Gattens, W.S. Meng, A cationic peptide consists of ornithine and histidine repeats augments gene transfer in dendritic cells, Mol. Immunol. 40 (2003) 483–490.

[37] M.Y. Ono, E.M. Spain, Dynamics of DNA condensates at the solid-liquid interface by atomic force microscopy, J. Am. Chem. Soc. 121 (1999) 7330–7334.

[38] A.L. Martin, M.C. Davies, B.J. Rackstraw, C.J. Roberts, S. Stolnik, S.J.B. Tendler, P.M. Williams, Observation of DNA-polymer condensate formation in real time at a molecular level, FEBS Lett. 480 (2000) 106–112.

[39] T. Okuda, S. Kidoaki, M. Ohsaki, Y. Koyama, K. Yoshikawa, T. Niidome, H. Aoyagi, Time-dependent complex formation of dendritic poly(L-lysine) with plasmid DNA and correlation with in vitro transfection efficiencies, Org. Biomol. Chem. 1 (2003) 1270–1273.